HiSST: 3rd International Conference on
High-Speed Vehicle Science Technology
14 -19 April 2024, Busan, Korea

Numerical Simulation of Multi-Temperature Thermochemical Non-Equilibrium Model Over High Enthalpy Flow

Chanho Kim[1], Yosheph Yang[2], Jae Gang Kim[3], Kyu Hong Kim[4]

Abstract (Tahoma 11 pt, bold)

In hypersonic computational fluid dynamics studies, using a two-temperature model to simulate thermochemical non-equilibrium states is common. The two-temperature model assumes translational-rotational, electron-electronic-vibrational temperatures and includes the assumption that each energy has an equal temperature. In this study, the temperature of each energy mode was separated and the effects were analyzed. The three-temperature model uses translational-rotational, vibrational, and electron-electronic temperatures by independently calculating the electron-electronic temperature from the two-temperature model. The four-temperature model calculated the rotational temperature independently. To accurately calculate the electron-electronic temperature, not only the Lee model but also the Laporta model was used to model the e-V relaxation time of N_2, O_2, NO. The validation of the multi-temperature model solver was performed by comparing the heat flux of ELECTRE, LENS-XX experiments, and the electron number density of RAM-C. The effect of the multi-temperature model is most pronounced in the wake region, where the flow expands and affects the formation of ions and electrons.

Keywords: Hypersonic, Non-Equilibrium, Computational Fluid Dynamics, Electron-Electronic Temperature, Electron Number Density

Nomenclature

ρ – density
u, v – velocity components in the x and y directions
e – internal energy
p – pressure
h – total enthalpy
τ – shear stress
q – conduction term
$\dot{\omega}$ – species production rate
S – nonequilibrium source
J – diffusion velocity
Superscripts
x, y – x, y coordinates component
Subscripts
$trans$ – Translational
rot – Rotational
vib – Vibrational
ee – Electron-Electronic
s – species s

1. Introduction

The hypersonic aerothermodynamic field is focused on 2-T models. Simulation of real gas effect using 2-T models of air has been widely studied in the past. Recently, new TPS models utilizing electrons [1] have been developed to accurately capture the blackout phenomenon during reentry to Earth. For these studies utilizing electrons, it is important to accurately capture the electron number density, so it is necessary to consider each energy mode individually to see how it affects the heat transfer of the gas

[1] *Seoul National University, 1, Gwanak-ro, Gwanak-gu, Seoul 08826, Republic of Korea, nahcho@snu.ac.kr*
[2] *Kangwon National university, 1, Kangwondaehak-gil, Chuncheon-si, Gangwon-do 24341, Republic of Korea, yyang@kangwon.ac.kr*
[3] *Sejong University, 209 Neungdong-ro, Seoul 05006, Republic of Korea, jaegkim@sejong.ac.kr*
[4] *Seoul National University, 1, Gwanak-ro, Gwanak-gu, Seoul 08826, Republic of Korea, aerocfd1@snu.ac.kr*

and the flow field around the gas, which is incorporated as an assumption of the traditional two-temperature model. Recently, studies related to rotational relaxation time [2] and e-V energy exchange [3, 4] have been conducted. In this study, by applying the latest models, a more accurate multi-temperature model was constructed and the effects of each temperature model were analyzed.

2. Methodology

The governing equations of the 4-T, 3-T, and 2-T models used in the multi-temperature model are shown below. The 4-T model separates the translational, rotational, vibrational, and electron-electronic energies and considers all energy transitions between each energy to obtain the temperature. The 3-T model ignores the energy transition between translational and rotational energy, assuming that the translational and rotational temperatures have the same temperature. The 2-T model ignored energy transitions between vibrational and electron-electronic energy, including the assumption that the vibrational temperature is the same as the electron-electronic temperature in the assumptions of the 3-T model. The energy transitions between each energy in the 4-T, 3-T, and 2-T models are summarized in Fig 1. The governing equations of the multi-temperature model are summarized in Sections 2.1, 2.2, and 2.3.

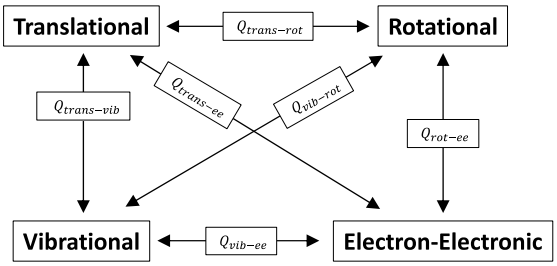

Fig 1. Considered Energy Relaxation Terms of Energy Modes

2.1. 4-Temperature Model

$$Q = \begin{pmatrix} \rho_s \\ \rho u \\ \rho v \\ \rho e \\ \rho e_{rot} \\ \rho e_{vib} \\ \rho e_{ee} \end{pmatrix}, E = \begin{pmatrix} \rho_s u \\ \rho uu + p \\ \rho uv \\ \rho hu \\ \rho e_{rot} u \\ \rho e_{vib} u \\ \rho h_{ee} u \end{pmatrix}, E_v = \begin{pmatrix} -J_{s,x} \\ \tau_{xx} \\ \tau_{xy} \\ u\tau_{xx} + v\tau_{xy} - (q^x) \\ -(q^x_{rot}) \\ -(q^x_{vib}) \\ -(q^x_{ee}) \end{pmatrix}, S = \begin{pmatrix} \dot{\omega}_s \\ 0 \\ 0 \\ 0 \\ S_{rot} \\ S_{vib} \\ S_{ee} \end{pmatrix} \quad (1)$$

2.2. 3-Temperature Model

$$Q = \begin{pmatrix} \rho_s \\ \rho u \\ \rho v \\ \rho e \\ \rho e_{vib} \\ \rho e_{ee} \end{pmatrix}, E = \begin{pmatrix} \rho_s u \\ \rho uu + p \\ \rho uv \\ \rho hu \\ \rho e_{vib} u \\ \rho h_{ee} u \end{pmatrix}, E_v = \begin{pmatrix} -J_{s,x} \\ \tau_{xx} \\ \tau_{xy} \\ u\tau_{xx} + v\tau_{xy} - (q^x) \\ -(q^x_{vib}) \\ -(q^x_{ee}) \end{pmatrix}, S = \begin{pmatrix} \dot{\omega}_s \\ 0 \\ 0 \\ 0 \\ S_{vib} \\ S_{ee} \end{pmatrix} \quad (2)$$

2.3. 2-Temperature Model

$$Q = \begin{pmatrix} \rho_s \\ \rho u \\ \rho v \\ \rho e \\ \rho e_{eev} \end{pmatrix}, E = \begin{pmatrix} \rho_s u \\ \rho uu + p \\ \rho uv \\ \rho hu \\ \rho h_{eev} u \end{pmatrix}, E_v = \begin{pmatrix} -J_{s,x} \\ \tau_{xx} \\ \tau_{xy} \\ u\tau_{xx} + v\tau_{xy} - (q^x) \\ -(q^x_{ee} + q^x_{vib}) \end{pmatrix}, S = \begin{pmatrix} \dot{\omega}_s \\ 0 \\ 0 \\ 0 \\ S_{ee} + S_{vib} \end{pmatrix} \quad (3)$$

The governing equations for 2-T and 3-T can be found by adding the rows of the governing equation of 4-T. The source term in the 4-T basis is constructed as follows. In Eq. (4), (5) and (6), the source terms added compared to 2-T are S_{trans-rot}, S_{e-vib}. The $S_{trans-rot}$ term uses the relaxation model of Jo [2], and the S_{e-vib} term uses the model of Lee [5] for N_2 and Laporta [3,4] for O_2, NO.

$$S_{rot} = S_{trans-rot} - S_{rot-e} + S_{vib-rot} + S_{Chem-rot} \quad (4)$$

$$S_{vib} = S_{trans-vib} - S_{vib-rot} + S_{e-vib} + S_{Chem-vib} \quad (5)$$

$$S_{ee} = S_{trans-e} + S_{rot-e} - S_{e-vib} + S_{Chem-ee} \quad (6)$$

3. Results

RAM-C II [6] is a 1.3m long sphere-cone consisting of a 0.152m diameter sphere and a $9°$ cone. The RAM-C II experiment was conducted to measure the electron number density around a hypersonic vehicle during reentry. This study analyzes the 71 km altitude conditions of RAM-C II. The 71 km altitude is the condition where the reflectometer measurements are most similar to the actual values.

The result of the 4-T, 3-T, and 2-T models at 71km altitude is shown in Fig 2. Fig 2 shows the maximum electron number density in the direction normal to the wall, which confirms the small discrepancy with the experimental results. Compared to the 2-T and 3-T models, the 4-T model shows a slightly lower electron number density, which seems to be caused by an increase in the shock standoff distance due to the effect of rotational relaxation during shock wave formation.

The experimental data from the electrostatic probe for the rear of the gas and the predictions from the multi-temperature model are compared in Fig. 3. All models predicted the electron number density within the error. The electron temperature in the wake region is shown in Fig. 4. The difference between 2-T and 4-T was largest in the recirculation region where the separation occurred, and equilibrium was reached further downstream. To see the difference between the multi-temperature models, the electron number density was compared with the temperature of the same streamline. The comparison of temperature and electron number density for the multi-temperature models is shown in Fig. 5. The most significant differences are seen in 3-T and 4-T, where electron-electronic nonequilibrium is considered. This shows the need for electron-electronic nonequilibrium for accurate electron-electronic temperature prediction due to the relatively long relaxation time characteristic of the electron-electronic temperature, unlike the vibrational temperature, which quickly reaches equilibrium with the translational temperature.

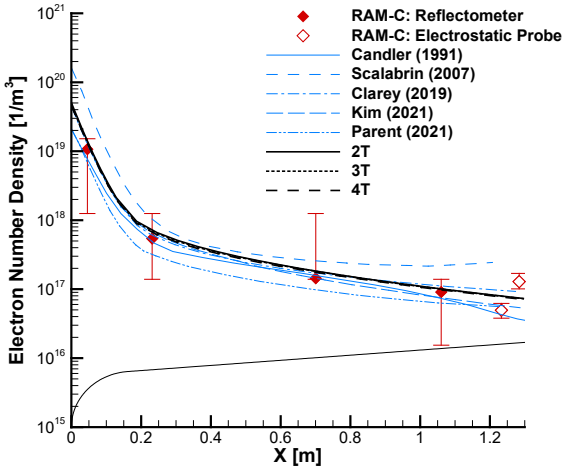

Fig 2. Comparison of maximum electron number density perpendicular to the wall of the RAM-C II flight test condition 71 km with experimental data and other studies

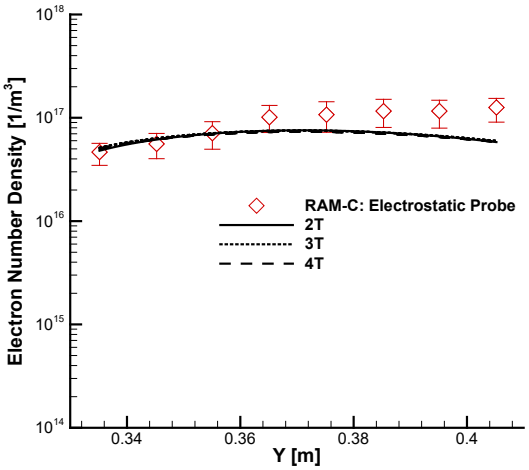

Fig 3. Comparison of electron number density at the electrostatic probe of multi-T models with experimental data from the RAM-C II flight test 71 km

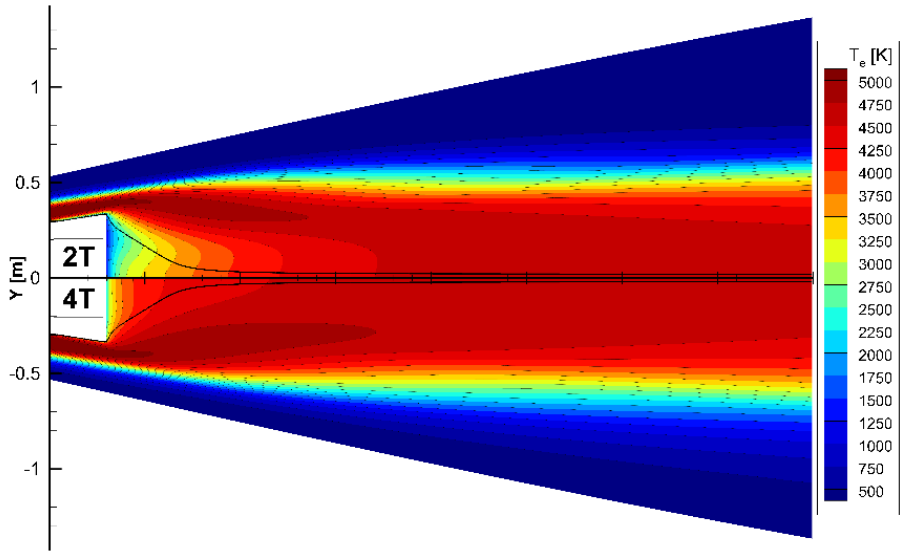

Fig 4. Comparison of electron temperature distribution of 2-T and 4-T in wake region at 71km altitude of RAM-C II flight test condition

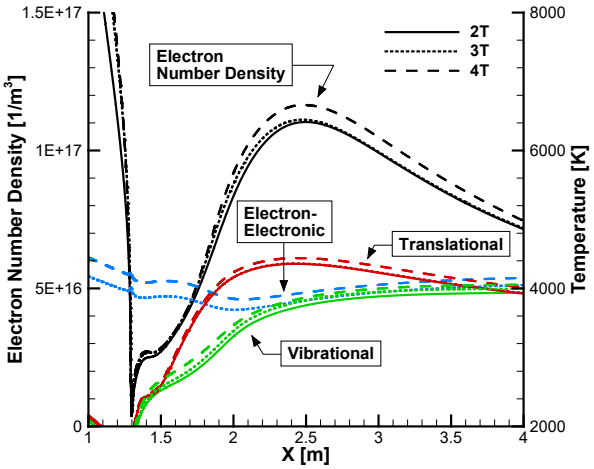

Fig 5. Comparison of temperature and electron number density along streamline in wake region at 61km altitude of RAM-C II flight test condition

ELECTRE [5] is a 2m long sphere-cone with a 0.175m diameter sphere and a cone with $4.6°$. ELECTRE has published flight test data, allowing for a direct comparison of heat transfer. As shown in Fig 6, the analysis of each multi-temperature model shows that the difference between the 2-T and 3-T models is very small, but the 4-T model shows a slight decrease in heatflux.

The stagnation line temperature distributions at 293 s for the multi-temperature models are compared in Fig. 7. Compared to the previous RAM-C II case, the nonequilibrium regions of T_{vib} and T_{ee} increased significantly, but T_{trans} and T_{rot} reached equilibrium quickly. The flight condition of ELECTRE is a low-altitude, low-enthalpy condition compared to RAM-C II, and the maximum electron number density in the stagnation line is reduced by two orders of magnitude. Therefore, the effect of rotational nonequilibrium is greatly reduced, and the $e - vib$ relaxation transfer is also reduced due to the reduction of electron production rate.

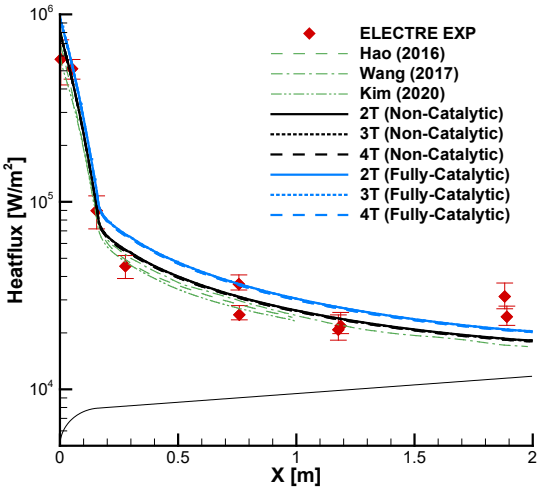

Fig 6. Heat Flux Comparison of Multi-Temperature Models of ELECTRE 293s condition

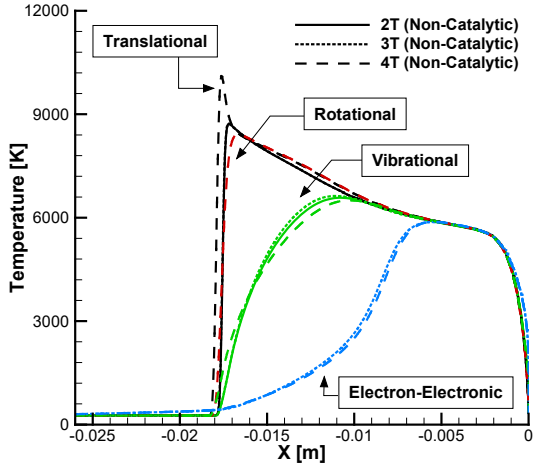

Fig 7. Comparison of temperatures along stagnation line of ELECTRE

For the LENS-XX experiment [7], the analysis was performed for 2-T, 3-T, and 4-T models. The results of the LENS-XX analysis for multi-temperature model showed similar to the previous analysis.

The heat flux of the hemisphere and cylinder and the temperature distribution of the stagnation line are compared in Fig. 7 and 8. Similar to the previous case, we can see that the differences between the multi-temperature models are negligible. The same trend is observed for the differences between 3-T and 4-T compared to 2-T of the stagnation line.

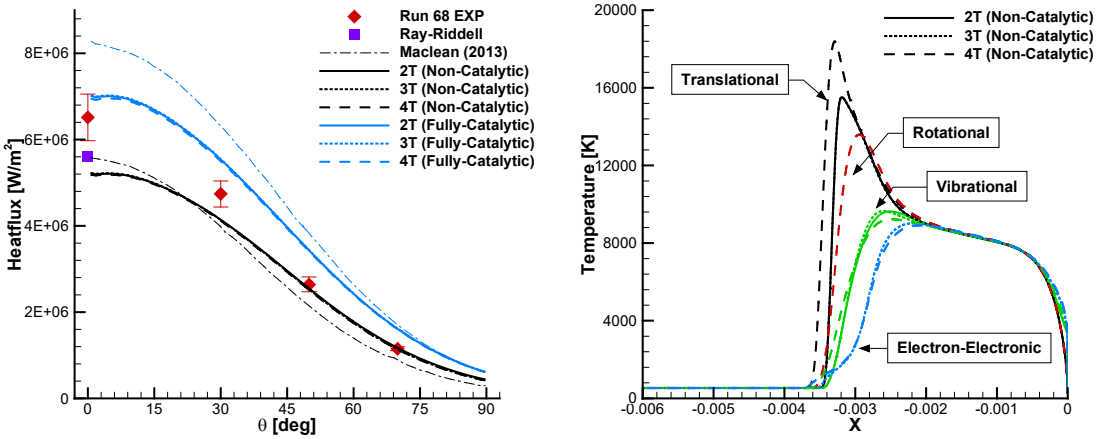

Fig 8. Comparison of surface heat flux and temperatures distribution along stagnation line of LESN-XX Hemisphere Run 68

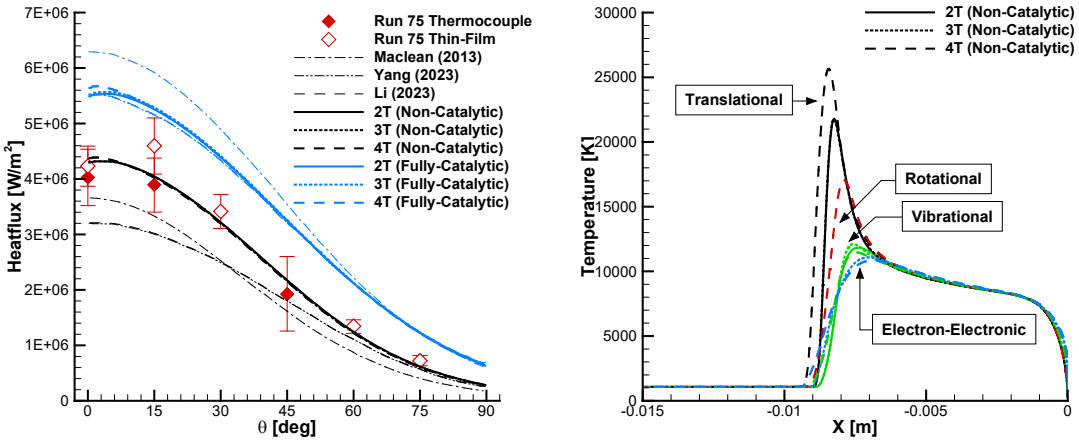

Fig 9. Comparison of surface heat flux and temperatures distribution along stagnation line of LESN-XX Cylinder Run 74

4. Conclusions

In this study, the numerical simulation results of 4-T, 3-T, and 2-T models were compared with the experimental results of RAM-C II, ELECTRE and LENS-XX to analyze the effect of the multi-temperature model in hypersonic flow. The 2-T and 3-T models showed less difference in the wall heatflux and the electron number density in the flow compression region. However, in the wake region, the 3-T and 4-T model predicted a higher electron-electronic temperature than the 2-T model due to the relatively long $e - vib$ relaxation time. The 4-T model tends to over-predict electron number density in wake region.

References

1. Hanquist, Kyle M., and Iain D. Boyd.: Plasma Assisted Cooling of Hot Surfaces on Hypersonic Vehicles. Frontiers in Physics 7, 9 (2019)
2. Jo, S. M., Panesi, M., and Kim, J. G.: Prediction of shock standoff distance with modified rotational relaxation time of air mixture. Physics of Fluids, 33(4). (2021). https://doi.org/10.1063/5.0045842
3. Laporta, V., Heritier, K. L., and Panesi, M.: Electron-vibration relaxation in oxygen plasmas. Chemical Physics, 472, 44–49. (2016). https://doi.org/10.1016/j.chemphys.2016.03.002
4. Laporta, V., Vialetto, L., and Guerra, V.: Vibrational excitation cross sections for non-equilibrium nitric oxide-containing plasma. Plasma Sources Science and Technology, 31(5). (2022). https://doi.org/10.1088/1361-6595/ac6a0f
5. Muylaert, J., Walpot, L., Haüser, J., Sagnier, P., Devezeaux, D., Papirnyk, O., and Lourme, D.: Standard model testing in the european high enthalpy facility f4 and extrapolation to flight. AIAA/ASME/SAE/ASEE 28th Joint Propulsion Conference and Exhibit, (1992).
6. Grantham, W. L.: Flight results of a 25000-foot-per-second reentry experiment using microwave reflectometers to measure plasma electron density and standoff distance. NASA Technical Note (TN). (1970).
7. MacLean, M., Marineau, E., Parker, R., Holden, M., Dufrene, A., and DesJardin, P.: Effect of surface catalysis on measured heat transfer in expansion tunnel facility. Journal of Spacecraft and Rockets, 50(2), 470–474. (2013). https://doi.org/10.2514/1.A32327